version January 15, 2022: fm
Preprint typeset using LaTeX style emulateapj v. 11/10/09

arXiv:2004.02969v2 [astro-ph.HE] 15 Apr 2020

DECIPHERING THE LARGE-SCALE ENVIRONMENT OF RADIO GALAXIES IN THE LOCAL UNIVERSE II. A STATISTICAL ANALYSIS OF ENVIRONMENTAL PROPERTIES

F. Massaro[1,2,3,4], A. Capetti[2], A. Paggi[1,2,3], R. D. Baldi[5],
A. Tramacere[6], I. Pillitteri[7], R. Campana[8], A. Jimenez-Gallardo[1,2] & V. Missaglia[9]

version January 15, 2022: fm

ABSTRACT

In our previous analysis we investigated the large-scale environment of two samples of radio galaxies (RGs) in the local Universe (i.e. with redshifts $z_{\rm src} \leq 0.15$), classified as FR I and FR II on the basis of their radio morphology. The analysis was carried out using i) extremely homogeneous catalogs and ii) a new method, known as *cosmological overdensity*, to investigate their large-scale environments. We concluded that, independently by the shape of their radio extended structure, RGs inhabit galaxy-rich large-scale environments with similar characteristics and richness. In the present work, we first highlight additional advantages of our procedure, that does not suffer cosmological biases and/or artifacts, and then we carry out an additional statistical test to strengthen our previous results. We also investigate properties of RG environments using those of the *cosmological neighbors*. We find that large-scale environments of both FR Is and FR IIs are remarkably similar and independent on the properties of central RG. Finally, we highlight the importance of *comparing radio sources in the same redshift bins* to obtain a complete overview of their large-scale environments.

Subject headings: surveys; methods: statistical; galaxies: active; galaxies: clusters: general; galaxies: jets; radio continuum: galaxies.

1. INTRODUCTION

In the last decades, extensive multifrequency investigations, combined with different statistical procedures, have shown that radio galaxies (RGs) preferentially inhabit galaxy-rich large-scale environments (see e.g., Prestage & Peacock 1988; Hill & Lilly 1991; Zirbel 1997; Worrall & Birkinshaw 2000; Belsole et al. 2007; Tasse et al. 2008), making them ideal laboratories to investigate formation and evolution of cosmological structures (see also Best 2004; Gendre et al. 2013; Ineson et al. 2013; Ineson et al. 2015). Most of these studies compare different classes of RGs, distinguishing between FR I (i.e, edge-darkened) and FR II (i.e, edge-brightened) classes (Fanaroff & Riley 1974) or between low excitation and high excitation RGs (LERGs and HERGS, respectively; see e.g., Hine & Longair 1979; Laing et al. 1994).

The most efficient approaches, that allows to get a complete overview of both galaxies and intergalactic medium (IGM) are certainly those based or combined with X-ray observations (see e.g., Hardcastle & Worrall 2000; Ineson et al. 2013; Ineson et al. 2015). Although in the last decades, thanks to XMM-*Newton* and *Chandra* campaigns, X-ray archives were enriched of RG observations (see e.g., Evans et al.2006; Croston et al. 2008; Massaro et al. 2012; Mingo et al. 2014; Massaro et al. 2015; Mingo et al. 2017; Massaro et al. 2018; Stuardi et al. 2018, for recent results), the largest fraction of the analyses carried out to date on their large-scale environments are preferentially based on optical and infrared surveys (see e.g., Ching et al. 2017; Miraghei & Best 2017; Massaro et al. 2019). This is mainly due to difficulties on performing deep and, at the same time, wide-area X-ray surveys, that would allow us to avoid biases introduced by a scarce sampling of RG populations. Results achieved to date are not always in agreement.

We recently proposed a different approach based on the selection of extremely homogenous datasets, restricted to the local Universe (i.e., source redshifts $z_{src} \leq 0.15$), to shed light on RG large-scale environments (Massaro et al. 2019, hereinafter M19).

We first created two extreme homogeneous catalogs of FR I and FR II RGs (hereinafter FRICAT and FRIICAT, respectively; Capetti et al. 2017a; Capetti et al. 2017b) at high level of completeness (i.e., $\sim$95%), based on uniform radio images available thanks to the Faint Images of the Radio Sky at Twenty cm (FIRST) radio survey (White et al. 1997; Helfand et al. 2015) that has almost the same footprint of the Sloan Digital Sky Survey (see e.g, Ahn et al. 2012) and is also completely covered by the NRAO VLA Sky Survey (NVSS; Condon et al. 1998) and, in the mid-infrared, thanks to observations of the Wide-field Infrared Survey Explorer (i.e., WISE; Wright et al. 2010). Then our investigation compared the efficiency of several clustering algorithms, including a new procedure, known as *cosmological overdensity*, based on the so-called *cosmological neighbors* (see the follow-

[1] Dipartimento di Fisica, Università degli Studi di Torino, via Pietro Giuria 1, I-10125 Torino, Italy.
[2] INAF-Osservatorio Astrofisico di Torino, via Osservatorio 20, 10025 Pino Torinese, Italy.
[3] Istituto Nazionale di Fisica Nucleare, Sezione di Torino, I-10125 Torino, Italy.
[4] Consorzio Interuniversitario per la Fisica Spaziale, via Pietro Giuria 1, I-10125 Torino, Italy.
[5] Department of Physics and Astronomy, University of Southampton, Highfield, SO17 1BJ, UK.
[6] University of Geneva, Chemin d'Ecogia 16, Versoix, CH-1290, Switzerland.
[7] INAF-Osservatorio Astronomico di Palermo G.S. Vaiana, Piazza del Parlamento 1, 90134, Italy.
[8] INAF/OAS, via Piero Gobetti 101, I-40129, Bologna, Italy.
[9] Harvard - Smithsonian Astrophysical Observatory, 60 Garden Street, 02138, Cambridge (MA), USA.

ing sections for more details), opportunely developed to avoid cosmological biases and artifacts.

We mainly concluded that RGs, independently of their radio (FR I vs. FR II) or optical classification (LERG vs. HERG) tend to inhabit galaxy-rich large-scale environments with similar richness (M19). However, the limited number of HERGs present in our FRIICAT prevented us from drawing firm statistical conclusions when comparing LERG and HERG populations, thus the statement based on the optical classification has to be treated with caution deserving a deeper analysis. Finally, we highlighted the importance of *comparing radio sources in the same redshift bins* to obtain a complete overview of their large-scale environments. It is worth highlighting that searching for galaxy clusters and groups using spectroscopic redshifts is a method already used in the past (see e.g., Danese et al. 1980; Hucra & Geller 1982; Girardi et al. 1993; Fadda et al. 1996).

Here we first present additional evidences of cosmological biases and artifacts that could affect analyses of the large-scale environments highlighting the advantages of the cosmological overdensity method. Then we perform an additional statistical test to obtain a direct comparison between the FR I and the FR II populations. On the basis of the distribution of optical sources surrounding RGs, we also present a new set of parameters to i) characterize and ii) compare their large-scale environments.

The paper is organized as follows. In § 2 we describe the samples selected to carry out our analysis while in § 3 we provide a brief description of the cosmological overdensity procedure. Additional evidences of cosmological biases and artifacts that could arise in similar analyses is given in § 4. Then in § 5 we present a new statistical test that strengthens the evidence that FR Is and FR IIs inhabit similar galaxy-rich large-scale environments, while § 6 is devoted to the description of several ambient parameters obtainable from the distribution of *cosmological neighbors*. § 7 is then dedicated on future developments achievable with dedicated X-ray observations. Finally, summary and conclusions are given in § 8 with tables and additional figures reported In Appendix A.

As in M19, we adopt cgs units for numerical results and we assume a flat cosmology with $H_0 = 69.6$ km s^{-1} Mpc^{-1}, $\Omega_{\rm M} = 0.286$ and $\Omega_\Lambda = 0.714$ (Bennett et al. 2014), unless otherwise stated. Thus, according to these cosmological parameters, $1''$ corresponds to 0.408 kpc at $z_{\rm src}$ =0.02 and to 2.634 kpc at $z_{\rm src}$ =0.15.

2. SAMPLE SELECTION

We selected two RG catalogs to carry out our analysis starting from the radio-loud sample of Best & Heckman (2012).

The first catalog is the combination of FRICAT and sFRICAT both described in Capetti et al. (2017a). The FRICAT sources, chosen on the basis of their FR I radio morphology, are selected to have a radio structure beyond a distance of 30 kpc, measured from the optical position of the host galaxy, with the only exceptions of the 14 sFRICAT objects with radio extended emission having the same morphology but extending between 10 and 30 kpc but limited to z_{src} =0.05 (see Capetti et al. 2017a, for details). This combination of these two samples includes RGs at redshift $z_{src} \leq 0.15$, all hosted in red early-type galaxies and spectroscopically classified low excitation radio galaxies (LERGs) for a total of 209 radio sources.

The second sample is the FRIICAT (Capetti et al. 2017b), composed of 105 edge-brightened radio sources (FR II type) within the same redshift range of the previous catalog. About ∼90% of the FR IIs listed in the FRIICAT are spectroscopically classified as LERGs, being hosted red early-type galaxies as occurs for FR Is. The remaining ∼10% of the FRIICAT shows indeed optical spectra typical of high excitation radio galaxies (HERGs) and host galaxies bluer in the optical band and redder in the infrared than FR II LERGs.

Thanks to their selection criteria both RG catalogs are not contaminated by compact radio objects, as compact steep spectrum sources and FR 0s (Baldi et al. 2015; Baldi et al. 2018), which show a different cosmological evolution, with respect to FR Is and FR IIs and could potentially lie in different environments.

The selected RG catalogs include only sources lying in the central footprint of the SDSS, because it is the same sky area covered by the main catalog of groups and clusters of galaxies adopted in our analysis: the one created by Tempel et al. (2012, hereinafter T12). The T12 catalog has the largest number of cluster/group detections with spectroscopic redshifts $z_{\rm cl}$ in the range between 0.009 and 0.20 and peaking around 0.08. This catalog of groups and clusters is based on a modified version of the Friends-of-Friends algorithm (Hucra & Geller 1982; Tago et al. 2010) and its richness is indicated as N_{gal}.

3. COSMOLOGICAL OVERDENSITY

Our analysis on the large-scale environment of RGs is based on the definition of two type of optical sources lying within 2 Mpc. These are the i) cosmological neighbors and the ii) candidate elliptical galaxies whose definition is reported below, for sake of completeness.

1. *Cosmological neighbors:* all optical sources lying within the 2 Mpc radius computed at $z_{\rm src}$ of the central radio galaxy with all the SDSS magnitude flags indicating a galaxy-type object (i.e., *uc*=*rc*=*gc*=*ic*=*zc*=3), and having a spectroscopic redshift z with $\Delta\, z = |z_{\rm src} - z| \leq 0.005$, corresponding to the maximum velocity dispersion in groups and clusters of galaxies (see e.g., Moore et al. 1993; Eke et al. 2004; Berlind et al. 2006).

We indicate the number of cosmological neighbors, N_{cn}^{500}, N_{cn}^{1000} and N_{cn}^{2000}, lying within 500 kpc, 1 Mpc and 2 Mpc distance from the central radio galaxy, respectively, that provide an estimate of the environmental richness.

2. *Candidate elliptical galaxies:* all SDSS sources, lying within the 2 Mpc distance from the central RG at $z_{\rm src}$ and with $u - r$ and $g - z$ optical colors consistent with those of a sample of elliptical galaxies, chosen out of the galaxy zoo project (Lintott et al. 2008), at the same redshift and within the 90% level of confidence evaluated using the Kernel Density Estimator (Richards et al. 2004; D'Abrusco et al. 2009; Massaro et al. 2011; Massaro et al. 2013).

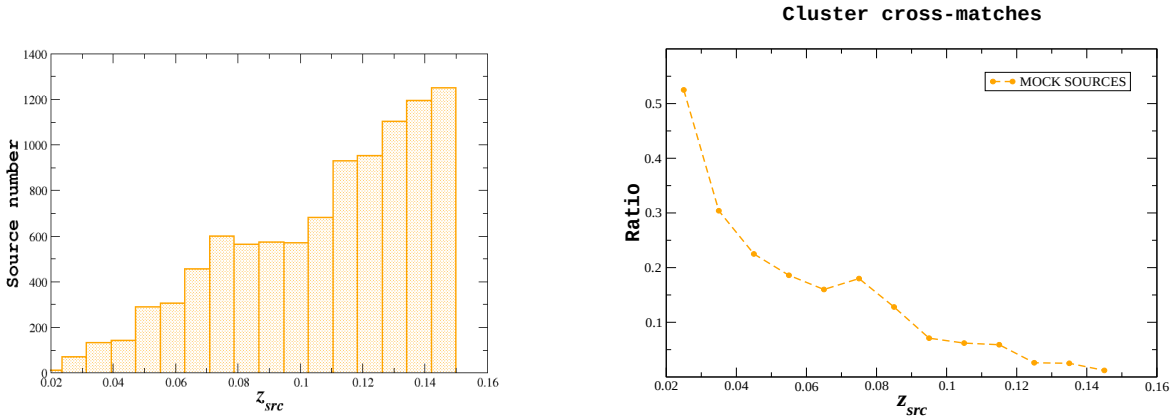


FIG. 1.— Left panel) The z_{src} distribution of 9800 random positions (i.e., mock sources) chosen in the SDSS footprint, lacking a radio counterpart within 5″. Right panel) The ratio between the number of mock sources having a group or a cluster of galaxies with richness $N_{gal} > 4$ from the T12 catalog and with having $\Delta z = |z_{\rm src} - z_{\rm cl}| \leq 0.005$, and the total number of mock sources in bin of z_{src} of size 0.01. This confirms our previous results based on a mock catalog of 5000 sources (Massaro et al. 2019) that it is easier to find a positive cross-match at low z_{src}.

We selected elliptical-type galaxies because their density in galaxy groups or clusters is larger than that of spirals (see e.g., Biviano 2000).

Source selected as candidate elliptical galaxies do not necessarily have spectroscopic $z_{\rm src}$ estimates.

Candidate elliptical galaxies were mainly used in the previous analysis with the following two aims. First, they allow to check galaxy rich environments also when the number of cosmological neighbors is limited, since we were able to test the presence of the "red sequence" (i.e., the well-known relation between colors and magnitude for galaxies that are members of groups and/or clusters Visvanathan & Sandage; Gladders et al. 1998; Gladders et al. 2000) with two different color magnitude diagrams (see M19 for more details). Then the distance between the 5^{th} candidate elliptical galaxy and the central RG was used to compute the Σ_5 parameter as an estimator of the richness (see e.g., Sabater et al. 2013; Worpel et al. 2013; Haas et al. 2012).

Based on our criterion, a cosmological overdensity occurs when the number of cosmological neighbors counted within 500 kpc is higher than the 95% quantile of the N_{cn}^{500} distribution measured for a sample of mock sources located in random positions of the sky. This N_{cn}^{500} threshold has been chosen in bin of $z_{\rm src}$ of size 0.01 to compare sources at same redshifts thus to avoid cosmological biases and artifacts. At redshifts above 0.1 we imposed to have at least two cosmological neighbors within 1 Mpc in addition to the previous criterion on N_{cn}^{500}. Additional and more specific details about this procedure can be found in M19.

4. COSMOLOGICAL BIASES AND ARTIFACTS

Here we describe several cosmological biases and artifacts encountered while carrying out our investigation to highlight advantages of using, whenever possible, the method of cosmological overdensity.

4.1. *Biases in the catalog crossmatches*

Cross-matches with catalogs of groups and clusters of galaxies shows a clear z_{src} dependence. As shown in Fig. 1, we built a sample of 9800 random positions in the SDSS footprint and cross-matched it with the T12 catalog. The redshift distribution of mock sources rises up to z_{src} =0.15 as those of FRICAT and FRIICAT.

The fraction of mock sources per redshift bin of size 0.01 having a positive crossmatch with a group or a cluster of galaxies within 2 Mpc, computed a its z_{src}, and having $\Delta z = |z_{\rm src} - z_{\rm cl}| \leq 0.005$ and $N_{gal} > 4$, significantly decreases while z_{src} increases. This indicates that we could expect a higher chance of finding a low redshift RG associated with a group or a galaxy cluster than a high redshift one. Thus we chose the thresholds on the number of cosmological neighbors in the cosmological overdensity as function of z_{src}.

A second problem arises when using catalog cross-matches regarding the richness estimated. In Fig. 2 we show the difference ΔN between the number of cosmo-

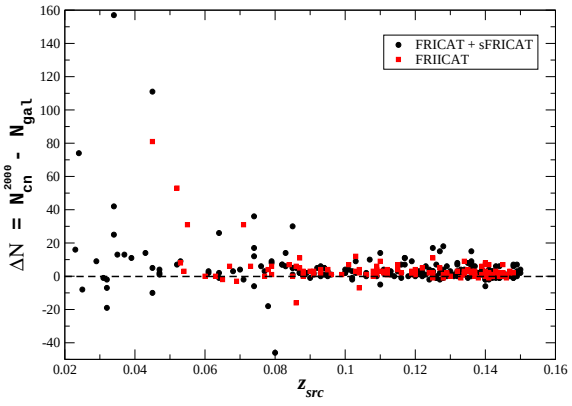


FIG. 2.— The difference ΔN between the number of cosmological neighbors, N_{cn}^{2000} lying within 2 Mpc distance from the central RG and N_{gal} the richness estimated in the T12 cluster catalog. Black circles mark radio sources in the FRICAT, including those of the sFRICAT, while red squares correspond to the FR IIs.

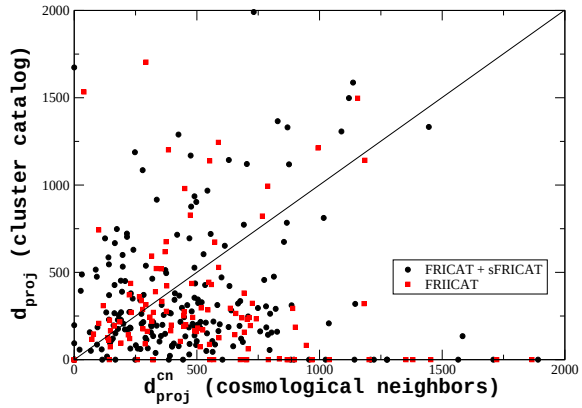


FIG. 3.— On the x axis we report the projected distance d_{proj} measured between the position of the RG in the center of the field examined and the centroid of the spatial distribution of cosmological neighbors within 2 Mpc while on the y axis the projected distance is computed using the location of the closest group/cluster positionally associated with the T12 catalog. As in Fig. 2 black circles mark radio sources in the FRICAT, including those of the sFRICAT, while red squares correspond to the FR IIs.

logical neighbors, N_{cn}^{2000} lying within 2 Mpc distance from the central RG and N_{gal} from the T12 group/cluster catalog. It is quite evident that the N_{gal} parameter underestimates the group/cluster richness. There are only a few cases where N_{cn}^{2000} provides a lower estimate of the group/cluster richness. However, these cases could be also due to an incorrect run of the algorithm of the T12 catalog since we did not detect sources lying at similar redshift of the central RG and not even candidate elliptical galaxies for most of them. It is worth noting that the richness estimated in cluster catalogs is generally decreasing with redshift, as for example occurs for N_{gal} in the T12, thus expecting to find less galaxy-rich environments as z_{src} increases.

Additional advantages of the method based on the cosmological overdensity with respect to the cluster catalog crossmatches regard the estimate of the position of the central RG with respect to cluster center both in angular separation and redshift. In Fig. 3 we show the projected distance d_{proj} measured between the position of the RG in the center of the field examined and i) the centroid of the spatial distribution of cosmological neighbors within 2 Mpc (x-axis) or ii) that of the group/cluster reported in the T12 catalog (y-axis). The majority of sources have values below bisector indicating that d_{proj} estimated via cosmological neighbors tend to be smaller than those evaluated with the T12 catalog.

Finally, in Fig. 4 we show the redshift difference Δz between the central RG z_{src} and i) the average value of the of cosmological neighbors lying within 2 Mpc (x-axis) and ii) the redshift of the closest cluster associated using the T12 catalog (y-axis). Once again the largest fraction of RG in both FRICAT and FRIICAT lies below the bisector, highlighting that cosmological neighbors provide a better sampling of the RG large-scale environment. Assuming that all RGs belong to a galaxy group/cluster, thanks to the distribution of cosmological neighbors we can achieve a better estimate of its redshift: $z_{\rm cl}$.

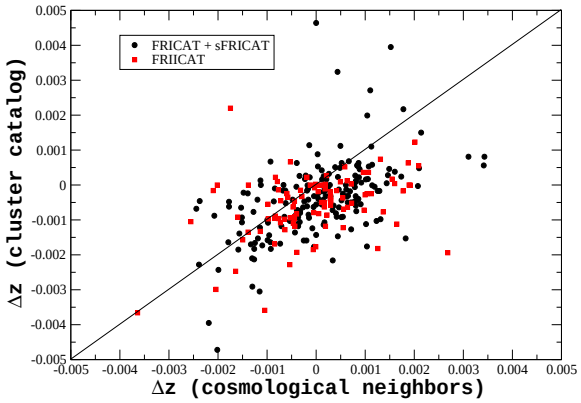


FIG. 4.— The redshift difference Δz between the central RG z_{src} and the average value of the of cosmological neighbors lying within 2 Mpc (x-axis) in comparison with that estimated using the spectroscopic redshift of the closest cluster associated with the T12 catalog (y-axis). Sources belonging to both FRICAT and sFRICAT are shown as black circles while FR IIs as red squares.

4.2. *Cosmological dependences of noise*

Selecting candidate elliptical galaxies on the basis of their spectroscopic redshift, whenever possible, is more precise than for example performing a simple magnitude cut as to estimate the Abell environmental richness. Counting overdensity of optical sources within a certain distance in kpc and with apparent magnitude $m \leq m_{src} + 2$, with m_{src} being the apparent magnitude of the central radio source (see e.g., Hill & Lilly 1991), introduces a significant amount of noise due to background and foreground objects being counted. This occurs because the number of optical galaxies increases significantly with the magnitude as shown for example in Fig. 5 for the R band apparent magnitude of galaxy-type objects (i.e., uc=rc=gc=ic=zc=3) in the 2 Mpc field of the FR I SDSSJ073505.25+415827.5. Thus comparing overdensity of optical sources around RG lying at different z_{src} when having the same absolute magnitude, or simply at different apparent magnitudes, implies comparing sources with a different signal-to-noise ratio. This makes the comparison between source populations having a different redshift distribution and/or different apparent magnitude distribution and/or a similar intrinsic luminosity/absolute magnitude, as FR Is and FR IIs, challenging. This effect could be actually mitigated by counting number sources per unit of area, since at larger redshifts areas of same physical size appear smaller thus containing less background/foreground sources (i.e., less noise), but, on the other hand, it does not help since it introduces a cosmological dependence of the noise.

In addition, sources selected to be galaxies above a certain threshold of apparent magnitude do not necessarily belong to the same group or cluster of galaxies. In Fig. 6, we show the ratio between the total number of cosmological neighbors and that of optical

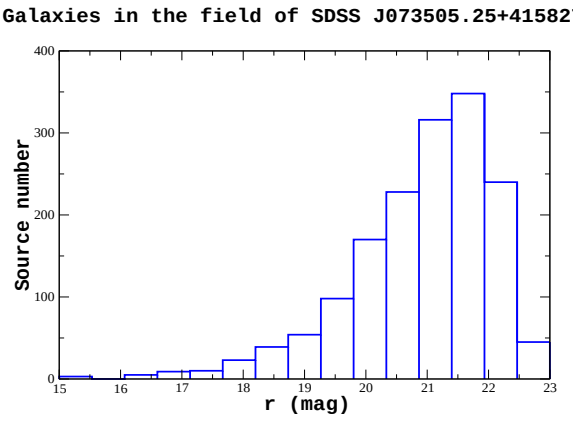


FIG. 5.— The distribution of the R band apparent magnitude r of all SDSS sources classified as galaxies (i.e., uc=rc=gc=ic=zc=3) in the 2 Mpc field of the FR I SDSSJ073505.25+415827.5. It is evident how the number of sources increases drastically when r increases up to the completeness level of the SDSS.

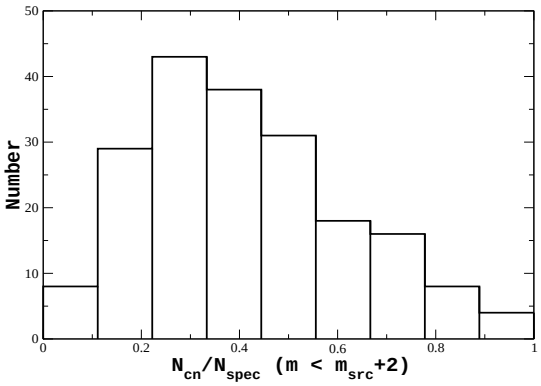


FIG. 6.— The distribution of the ratio between the total number of cosmological neighbors and that of optical sources with spectroscopic redshifts both selected to have $m \leq m_{src}+2$, in the R band, in the field of all FR Is lying within 2 Mpc form the central RG. This distribution shows how selecting sources only on the basis of their SDSS magnitude introduce more noise since out of those with a spectroscopic redshift only a tiny fraction, on average, appear to be gravitationally bounded with the central RG.

sources with spectroscopic redshifts both selected to have $m \leq m_{src}+2$ in the R band, similar to the definition of Abell classes (see e.g., Abell et al. 1989), within 2 Mpc distance from all FR Is listed in the FRICAT. Only 30-40% are generally lying at similar redshifts being so classifiable as cosmological neighbors, while others are simply background and foreground sources (i.e., noise), with very different redshifts, and thus erroneously counted. Noise-related effects related to the source selection with certain apparent magnitude can be partially mitigated by using photometric redshift estimates, as those provided in the SDSS, and counting sources on the basis of their absolute magnitudes and $V-R$ color (see e.g., Blanton et al. 2000; Blanton et al. 2001; Wing et al. 2011, and references therein), but not fully avoided. On the other hand, as shown in M19, the cosmological overdensity method does not suffer this noise effect since the threshold to indicate sources in a galaxy-rich large-scale environment is chosen as function of redshifts and because we compare RGs in the same redshift bin.

4.3. *Redshift evolution of the cosmological overdensity*

Here we show the underlying reason of adopting an "adaptive" procedure, as the cosmological overdensity method, with a threshold on the number of cosmological neighbors changing with redshift z_{src}.

In Fig 7 we show the 2 Mpc field around the FR I SDSS J160722.95+135316.4 at z_{src} =0.034, where red circles mark the locations of cosmological neighbors and dashed lines the distances of 1 Mpc and 2 Mpc, respectively. We computed the absolute magnitude in the R band of all cosmological neighbors and then maintaining their intrinsic power we rescaled them at larger distances, namely at redshifts 0.05, 0.10 and 0.15. We also recomputed the radii of the circles of 500 kpc, 1 Mpc and 2 Mpc at each redshift.

In each plot of Fig 7 we only reported those cosmological neighbors having the rescaled apparent magnitude m_r brighter than 17.8 corresponding to the SDSS criterion to select targets for spectroscopic observations. For the case of SDSS J160722.95+135316.4 the number of cosmological neighbors within 500 kpc (i.e., N_{cn}^{500}) decreases from 10 at z_{src} =0.034, to 3, 2 at z_{src} =0.05, 0.10 and none at z_{src} =0.15, resepctively, while N_{cn}^{2000} is actually 47 at 0.034 and 20, 4, 1 at z_{src} =0.05, 0.10, 0.15, respectively.

This suggests that the threshold chosen to indicate a galaxy-rich large-scale environment must be redshift dependent as we defined in our previous analysis on the basis of the MonteCarlo simulations performed on a large sample of random positions in the sky. We highlight that the above calculation does not take into account of any cosmological evolution of the groups or the clusters where RGs lie, it is a pure effect of the SDSS selection of spectroscopic targets that decreases the number of cosmological neighbors when the redshift increases as shown in our previous analysis (Massaro et al. 2019).

Finally, we also show in Fig 7 the number of optical galaxies with $m \leq m_{src}+2$, to highlight how the noise increases moving at higher redshift where the absolute magnitude of the central RG is fixed and it apparent magnitude m_{src} is rescaled.

5. STATISTICAL ANALYSES

To provide an additional evidence that the both FR Is and FR IIs live in galaxy-rich large-scale environment, we performed the following statistical tests all based on the number of cosmological neighbors N_{cn} surrounding them. It is worth noting that, as previously stated, the FRICAT used here is larger than the one adopted in our previous analysis since we also included the sFRICAT sample, allowing us to get a better sampling of the FR I population at lower redshifts.

The first test is based on the median of both FR I and FR II N_{cn} distributions. We computed median values of N_{cn}^{500} for FR Is (i.e., $\bar{N}_{cn}^{500}$), per bin of z_{src} of size 0.01, and then we compared the distribution of N_{cn}^{500} for FR IIs with $\bar{N}_{cn}^{500}$. We expect that if both RG populations live

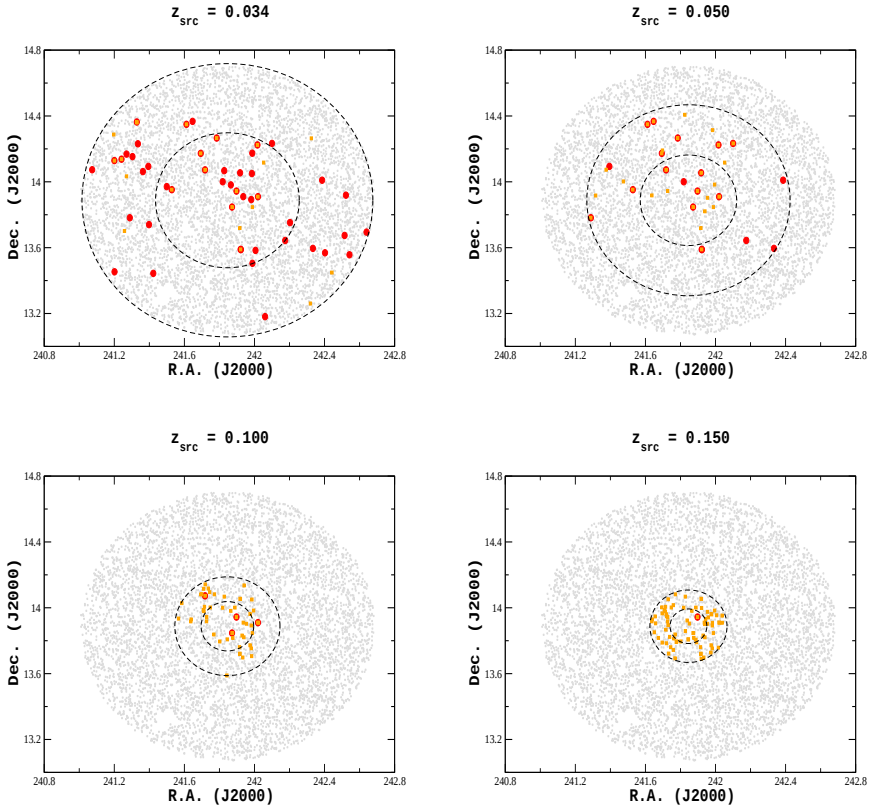


FIG. 7.— The spatial distribution of SDSS optical sources lying within 2 Mpc from the central RG at z_{src} =0.034 and having apparent magnitude in the R band greater than 19 shown as grey circles. Cosmological neighbors highlighted as red circles. Orange squares mark the location of optical galaxies with $m \leq m_{src} + 2$, to highlight how the noise increases moving at higher redshift. Dashed black lines refer to 1 Mpc and 2 Mpc distance from the central RG, respectively. In all other panels we show the distribution of cosmological neighbors computed assuming their intrinsic absolute magnitude M_r and rescaling their apparent magnitudes m_r at different redshifts, namely 0.05 (top right), 0.10 (bottom left) and 0.15 (bottom right), respectively. To create all plots at different redshifts than 0.034 we applied a cut for the rescaled apparent magnitude of the cosmological neighbors selecting only those brighter than 17.8. This limit corresponds to the SDSS criterion to select targets for spectroscopic observations. The number of cosmological neighbors decreasing when changing their distances maintaining the intrinsic power of their host galaxies strengthens our choice of having different thresholds at different redshifts to estimate cosmological overdensity.

in large-scale environment of similar richness, 50% of the FR IIs would lie above the median value computed for the FR Is while 50% below, for each bin of z_{src}. We also applied the same test to N_{cn}^{2000}. All medians values of both N_{cn}^{500} and N_{cn}^{2000} computed for the FR I population are reported in Table 1, together with the number of FR IIs that lie above and below the medians or having the same number of cosmological neighbors, per redshift bin.

For N_{cn}^{500}, in all 11 z_{src} bins explored, where we can compare FR Is and FR IIs, we found that in 4 cases the FR II median values are greater than $\bar{N}_{cn}^{500}$ computed for FR Is while in other 3 cases the situation is the opposite, and in all remaining cases medians of the two populations show the same medians. This is in agreement with the expectations of a binomial distribution, thus strengthening our results that, independently of their radio morphology, both classes of FR Is and FR IIs live in similar galaxy-rich large-scale environment. The median values $\bar{N}_{cn}^{500}$ for both population of FR Is and FR IIs are shown in Fig. 8. Then comparing $\bar{N}_{cn}^{2000}$ the situation is in agreement with previous results with 5 cases for which $\bar{N}_{cn}^{2000}$ of FR IIs is lower than that for the FR I population and 5 cases for which it is greater. Consequently, we can firmly confirm that the large-scale environments of the two classes of RGs, in each considered redshift range, is consistent.

Unfortunately, this first statistical test does not consider the two populations symmetrically, and it throws away almost all information about the distribution of environments present in the data. For example, if FR IIs has a systematically broader distribution of N_{cn} than FR Is, or a small tail of very rich, or very poor, environments, this first statistical test would be not sensitive to it. Thus, as second statistical check, we also applied the Mann-Whitney U rank test (a.k.a. Wilcoxon-Mann-Whitney test) to each redshift bin. In Fig. 8 we also report, above each value of the medians of the two RG distributions of N_{cn} the normalized z_U variable, defined as $\frac{U-E(U)}{\sigma_U}$), computed for the Mann-Whitney U test and this is always consistent with zero, as expected, within 2 σ level of confidence, with the only exception of a single bin between $z = 0.13$ and $z = 0.14$ where the number N_{cn} for the FR IIs appears systematically lower than the median of FR Is (see Table 1). It is worth noting that we did not apply this test at z <0.08 given the low num-

ber of FR IIs in these bins. Moreover, also this second statistical test is in agreement with our claim that the large-scale environments of FR Is and FR IIs cannot be distinguishable.

Then, for all redshift bins above 0.08 we also performed the two-sided Kolmogorov-Smirnov test between the distributions of N_{cn}^{500} and N_{cn}^{2000} of both FR Is and FR IIs, results on the D variable compute as well as correspondent p-values are reported in Table 2, where in agreement with previous tests and the null hypothesis that the two distributions are the same cannot be rejected.

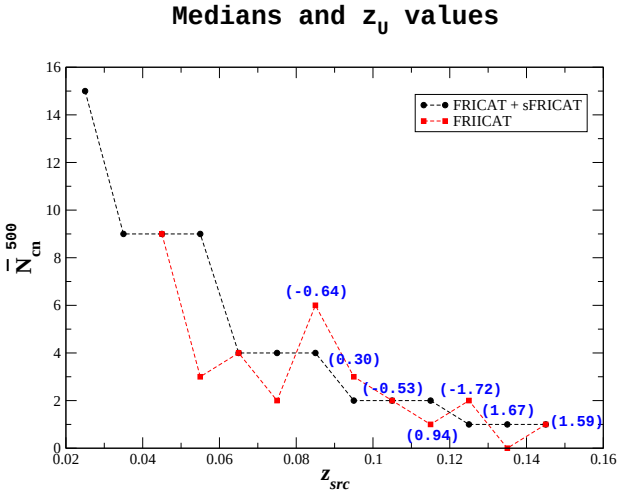


FIG. 8.— The median values for the FR I (black) and the FR II (red) RGs per bin of redshift z_{src}. Together with the median measurements of FR Is we also report the number of FR IIs that lie above and below them in red and for each z_{src} bin. As shown these fractions of FR IIs are almost equally distributed around the medians of the FR I population as expected for sources inhabiting similar large-scale environment, independently of their radio extended structure. Blue numbers reported in parenthesis above each median value, at all redshift bins above 0.08, correspond to values computed for the z_U normalized variable of the Mann-Whitney U rank test (see §. 5 for more details).

Finally, we verified that the shape of the two N_{cn} distributions with a third statistical check computing the skewness and the Pearson median skewness and verifying that the sign of both these parameters corresponds. This occurs in all redshift bins above 0.1 while below, due to the poor number of FR II radio galaxies in each z bin strongly affects both parameters providing not significant results. Again this last test provide results in agreement with the previous ones.

6. ENVIRONMENTAL PROPERTIES

6.1. *Environmental parameters: definition*

On the basis of the distribution of the cosmological neighbors it is possible to estimate several parameters to investigate the properties of the large-scale environments surrounding FR Is and FR IIs and compare them with those of the central RGs.

In particular, we defined the following quantities.

- The concentration parameter ζ_{cn}. It is defined as the ratio of the number of cosmological neighbors lying within 500 kpc and those within 1 Mpc. This parameter allows us to test if the RG tends to lie close to the center of the group or clusters of galaxies around it or in its outskirt. A similar concentration parameter has been estimate using candidate elliptical galaxies rather than cosmological neighbors: ζ_{el}.

- The average projected distance d_m^{cn} of the distribution of cosmological neighbors computed between their position and that of the central RG.

- The standard deviation σ_z of the redshift distribution of the cosmological neighbors surrounding each RG.

All values for the environmental parameters described above are also reported in Table 3 in Appendix.

6.2. *Environmental parameters: statistical analysis*

TABLE 1
COMPARISON BETWEEN $\bar{N}_{cn}^{500}$ AND $\bar{N}_{cn}^{2000}$ OF FR IS WITH FR IIS

z_{src}	$\bar{N}_{cn}^{500}$	N_{FRII} >< =	$\bar{N}_{cn}^{2000}$	N_{FRII} >< =
0.045	9	0 - 0 - 1	44	1 - 0 - 0
0.055	9	1 - 4 - 0	50	1 - 4 - 0
0.065	4	1 - 2 - 1	18	2 - 1 - 1
0.075	4	2 - 4 - 0	23	2 - 4 - 0
0.085	4	6 - 2 - 0	12	6 - 1 - 1
0.095	2	5 - 4 - 0	11	3 - 6 - 0
0.105	2	5 - 5 - 4	9	6 - 7 - 1
0.115	2	2 - 7 - 3	5	6 - 5 - 1
0.125	1	6 - 0 - 5	5	6 - 5 - 0
0.135	1	3 -10 - 4	8	1 -15 - 1
0.145	1	3 -14 -11	3	13 -13 - 2
total	-	34 - 52 - 29	-	47 - 61 - 7

Note: col. (1) report the central value of each redshift bin while col. (2) and col. (4) median values for the N_{cn}^{500} and N_{cn}^{2000} parameters computed for the FR I population and in comparison with the number of FR IIs (i.e., N_{FRII}) lying above (>), below (<) these median values of having being the same (=) as shown in col. (3) and col. (5), respectively.

TABLE 2
RESULTS OF THE TWO-SIDED KOLMOGOROV-SMIRNOV TEST RUN FOR THE FR I AND THE FR II DISTRIBUTIONS OF N_{cn}^{500} AND N_{cn}^{2000}.

z_{src}	D(N_{cn}^{500})	p(N_{cn}^{500})	D(N_{cn}^{2000})	p(N_{cn}^{2000})
0.085	0.289	0.804	0.337	0.629
0.095	0.291	0.760	0.368	0.469
0.105	0.232	0.816	0.223	0.851
0.115	0.172	0.986	0.235	0.831
0.125	0.296	0.499	0.269	0.622
0.135	0.224	0.650	0.382	0.084
0.145	0.205	0.445	0.089	0.999

Note: col. (1) report the central value of each redshift bin, while col. (2) and col. (4) the D statistical variable and col. (3) and col.(5) the correspondent p-value for the distribution of N_{cn}^{500} and N_{cn}^{2000}, respectively.

We investigated the distribution of the environmental parameters previously defined searching for possible trends with the RG properties, such as the absolute magnitude in the R band M_r, the radio luminosity L_R and the [OIII] emission line luminosity $L_{[OIII]}$.

The distribution of the concentration parameter ζ_{cn} for both FRICAT and FRIICAT is shown in Fig. 9. There are 52 FR Is out of 209 and 34 FR IIs out of a total 115, that have no cosmological neighbors within 500 kpc distance from their position. However this does not imply that their large-scale environment is not rich since it could be due, for example, to the SDSS spectroscopic incompleteness and/or to the position of the RG in the outskirt of its galaxy-rich large-scale environment. Most of the remaining RGs indeed appear to inhabit an environment with high galaxy density.

We note that the distribution of sources around a random position in the sky follows, in general, a uniform distribution, where the number of sources is expected to scale as $N \propto \vartheta^2$, with ϑ being the angular separation from the random position. Thus assuming that the same situation could be applicable to cosmological neighbors, the expected value of the ζ_{cn} is 0.25 while the largest fraction of the observed values is significantly higher.

In Fig. 10 we show the comparison between the concentration indices of FR Is computed using the number of cosmological neighbors ζ_{cn} and that of candidate elliptical galaxies ζ_{el}. The distribution of ζ_{el} is peaking around 0.4 and has the largest fraction of values in the range 0.2-0.6. There are less values around zero since it is "easier" to find candidate elliptical galaxies than cosmological neighbors due to the SDSS fiber cladding, which prevents fibers from being placed closer than 55″. A similar situation occurs for FR IIs.

We conclude that, independently of the concentration parameter adopted, RGs appear to inhabit galaxy-rich large-scale environments lying closer to the centroid of both cosmological neighbors and candidate elliptical galaxies.

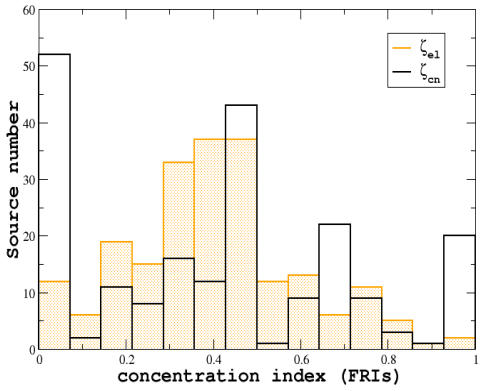


FIG. 10.— The comparison between the concentration indices computed using the number of cosmological neighbors ζ_{cn} (black) and that using candidate elliptical galaxies ζ_{el} (orange) for the FR I population. The main difference between the two distributions is the decreasing of the low values when using ζ_{el} with respect to ζ_{cn}. This is due to the fact that it is easier to find candidate elliptical galaxies with respect to cosmological neighbors. However, both parameters provide similar information.

Moreover, in Fig. 11 we also report the value of ζ_{cn} as function of the source redshift z_{src}. We do not see any trend/correlation between these two parameters and not even differences between the two RG classes.

Then we explore the distribution of the average projected distance d_m^{cn} of the distribution of cosmological neighbors and the standard deviation σ_z of their redshift distribution. These parameters provide an estimate of the group/cluster physical size. Their comparison is

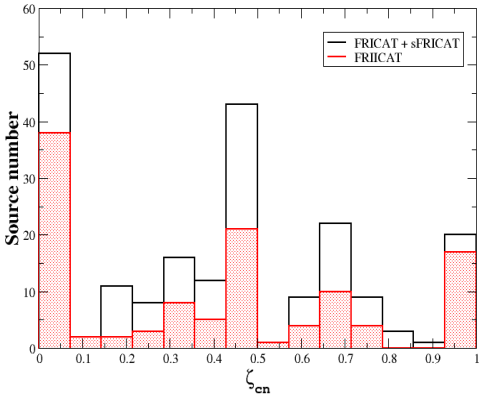


FIG. 9.— The distribution of the concentration parameter ζ_{cn} estimate using the distribution of the cosmological neighbors. Black histogram refers to the FR I population while the red one to the FR IIs. The two distributions for different RG classe are similar and the largest fraction of their values lie above the value of 0.25 expected assuming a uniform distribution of cosmological neighbors. Values of ζ_{cn} in the first bin (i.e., close to zero) are simply due to the lack of cosmological neighbors within 500 kpc distance from the central RG.

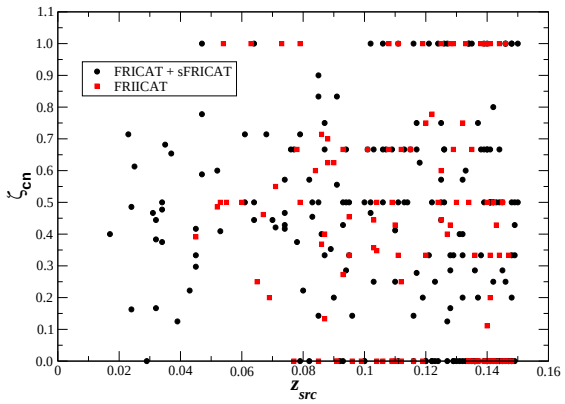


FIG. 11.— The concentration parameter ζ_{cn} as function of redshift z_{src} for both FR Is in black circles and FR II in red squares. No trend between these two parameters is evident thus we can claim that there is no cosmological evolution of the concentration parameter. Values of ζ_{cn} in the first bin (i.e., close to zero) are simply due to the lack of cosmological neighbors within 500 kpc distance from the central RG.

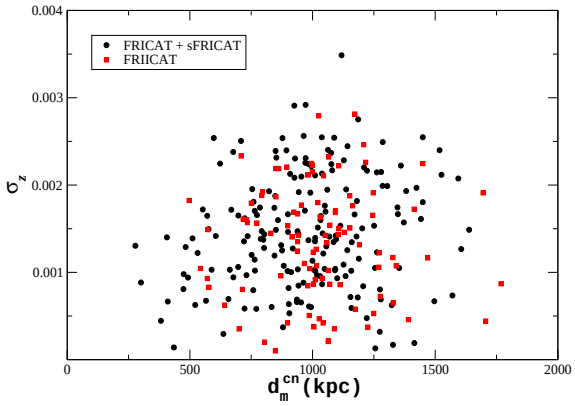


FIG. 12.— The comparison between the average projected distance d_m^{cn} of the distribution of cosmological neighbors and the standard deviation σ_z of their redshift distribution for both RG classes, namely: FR Is shown as black circles while FR IIs as red squares. No trend is evident between these two parameters.

shown in Fig. 12. We did not find any trend between these two parameters for both classes of RGs and as shown by their distributions in Fig. 13. In the latter case, we carried out a two-sided Kolmogorov-Smirnov test and we found the D parameter equal to 0.113 and corresponding to a p-value of 0.395 for a total number of 186 values of σ_z for the FR Is and 96 for the FR IIs, thus indicating that the null hypothesis that the two distributions are the same cannot be rejected. However, as

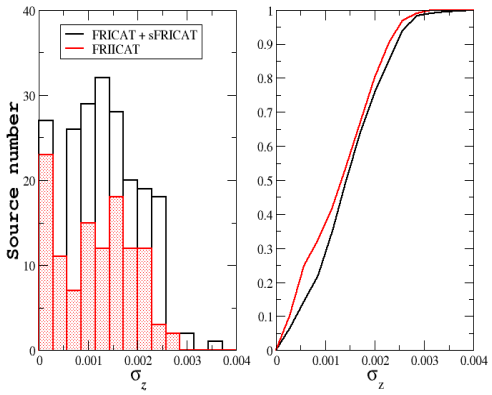


FIG. 13.— In the left panel we show the histogram of the standard deviation σ_z for redshift distribution of cosmological neighbors lying within 2 Mpc. Black histogram shows the behavior of FR Is while the red one that of FR IIs. Cumulative distributions, drawn from the binned histograms, are also shown in the right panel.

shown in Fig. 14, we found that for high values of N_{cn}^{2000} the redshift dispersion σ_z appear clustered around the 0.002.

In Fig. 15 we also show the values of both parameters, d_m^{cn} and σ_z, as function of z_{src} but no evidence of any trend is found.

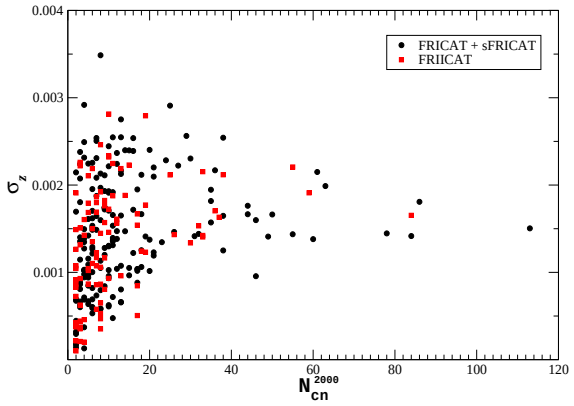


FIG. 14.— The comparison between the standard deviation σ_z of the redshift distribution of the cosmological neighbors and the number of cosmological neighbors within 2 Mpc: N_{cn}^{2000}, a parameter used to estimate the environmental richness. There is a trend between these two parameters, with environments with larger N_{cn}^{2000} appear to have larger values of σ_z. Black circles are referred to FR Is belonging to both the FRICAT and the sFRICAT while red squares mark FR IIs.

Finally, we explored other links between parameters of the central RG and those of the surrounding environments but no neat trends are evident. Figures are shown in Appendix.

We show d_m^{cn} and σ_z in comparison with the absolute magnitude in the R band of the RG where no trend/link is identified. A similar situation occurs also when comparing both these environmental parameters with radio power L_R and emission line luminosity of the [OIII], i.e., $L_{[OIII]}$. The plot with $L_{[OIII]}$ allows us also to test if there are differences between LERGs and HERGs, even if given the low number of HERGs present in our sample, these results must be treated with caution making this comparison less statistically significant. We conclude that independently by the power of the central RG in different energy range or that of its host galaxy the properties of its large-scale environment is the same, being independent by the radio morphology.

7. X-RAY PERSPECTIVES

We converted the standard deviation σ_z of the redshift distribution computed using all cosmological neighbors within 2 Mpc: N_{cn}^2000 into an estimate of the velocity dispersion σ_v of galaxies in the large-scale environments of radio galaxies. We computed the standard deviation of the line-of-sight component of the velocity (i.e. radial velocity) according to Danese et al. (1980), thus using the following relation:

$$v_{\parallel} = \frac{c(z_{src} - < z >_{cn})}{1 + < z >_{cn}} \qquad (1)$$

where z_{src} is the redshift of the central radio galaxy and $\bar{z}_{cn}$ is the average redshift of all cosmological neighbors within 2 Mpc. In Fig. 16 we show the distribution of the velocity dispersion computed on the basis of Eq. (1).

Then, considering σ_v, we also assumed that groups and clusters surrounding radio galaxies, being gravitationally bound, are virialized and thus we estimated the total

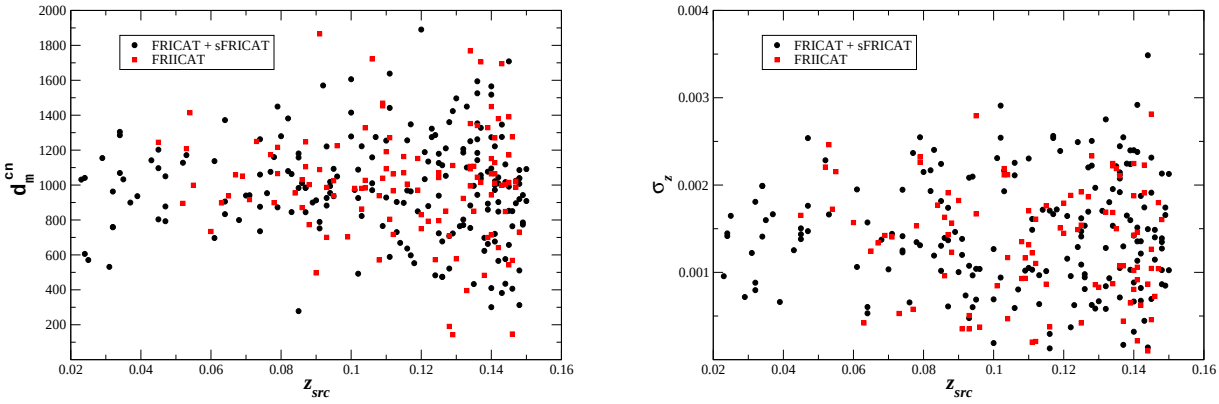


FIG. 15.— Left panel) the average projected distance d_m^{cn} of the distribution of cosmological neighbors vs. the redshift z_{src} of the central RG. Right panel) Same of the left panel for the σ_z parameter. FR Is are represented as black circles while FR IIs as red squares in both panels. No clear trend was found between these parameters and the RG redshift.

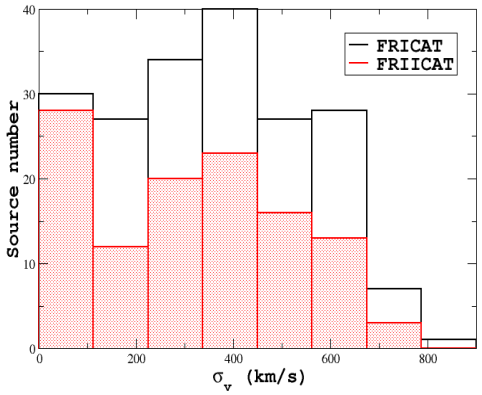


FIG. 16.— The distribution of the velocity dispersion for both FRICAT and FRIICAT sources derived according to Eq. (1). As expected from their their $sigma_z$ distribution, they are quite similar.

mass M_{env}, i.e. galaxies plus IGM plus dark matter content, for their large-scale environments, according to

$$M_{env} = \frac{\sigma_v^2 R_{vir}}{3G} \quad (2)$$

where we assumed R_{vir} =2 Mpc and we neglect the form factor 3/5.

We finally adopted two different correlations to estimate the X-ray luminosity L_X and the X-ray integrated flux F_X. The first correlation is

$$L_X = 3.3 \cdot 10^{26} \cdot M_{env}^{1.23} erg/s \quad (3)$$

as reported by Reiprich & Böhringer (1999) while the second directly links σ_v with the X-ray luminosity:

$$log\left(\frac{\sigma_v}{700\,km/s}\right) = -0.003 + 0.346 \cdot log\left(\frac{L_x\,E(z)^{-1}}{10^{44} erg/s}\right) \quad (4)$$

found by Clerc et al. (2016), where $E(z) = [(1+z_{src})^3 * \Omega_M + \Omega_\lambda]^{\frac{1}{2}}$.

Hence in Fig. 17 we show the distribution of the environmental mass M_{env} as well as that X-ray fluxes F_X estimated according to the previous relations and, using Eq. (3), as expected, they are all below the threshold of 4.4×10^{-12} erg/cm/s of the ROSAT Brightest Cluster Sample (Ebeling et al. 1998), while the same situation occurs for more than 95% of both radio galaxy catalogs when using Eq. (4). We remark that both L_X estimates are also consistent with those derived using the L_X vs σ_v correlation found by Zhang et al. (2011).

X-ray detection of the IGM emission in the large-scale environments of these radio galaxies depends on several issues (e.g., distribution of the surface brightness, X-ray background, size of the galaxy cluster etc.). However assuming that the X-ray integrated flux is uniformly spread over a circular region of 500 kpc radius centered on the central radio source, the mean values of the X-ray intensity we estimated ranges between 3-4e-16 and 1e-14 for both FR Is and FR IIs, respectively; typical values of galaxy clusters detected by satellites as *XMM-Newton* and *Chandra* (see e.g., Lloyd-Davies et al. 2011; Mehrtens et al. 2012).

Finally, we selected 2 FR Is out of 6 radio galaxies for which X-ray observations are available in the *XMM-Newton* archive and we carried out a simple analysis to show that low exposure times (∼5 ksec) can guarantee the X-ray detection of the IGM in galaxy cluster around them as well as in the majority of the sources in explored catalogs. Selected sources are: SDSS J113359.23+490343.4 and SDSS J120401.4+201356.3 and we cut the exposure times of their archival datasets to 5.5 ksec.

EPIC data were retrieved from the *XMM-Newton* Science Archive[10] and reduced with the SAS[11] 16.1.0 software. Following Nevalainen et al. (2005), we filtered XMM data for hard-band flares by excluding the time

[10] http://nxsa.esac.esa.int/nxsa-web
[11] http://www.cosmos.esa.int/web/*XMM-Newton*/sas

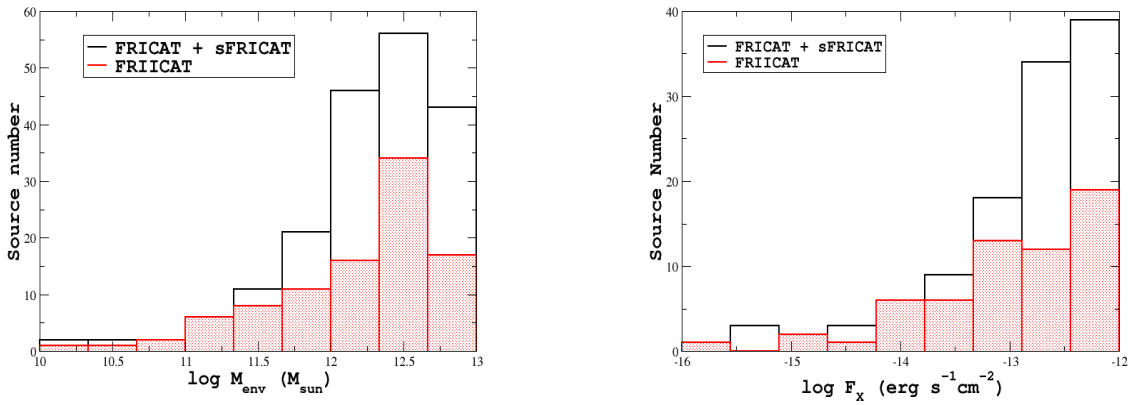


FIG. 17.— Left panel) The distribution of the environmental mass derived from the virial theorem. Right panel) The distribution of the integrated X-ray fluxes estimated from the velocity dispersion and the correlation of Eq. (3).

intervals where the high energy ($9.5-12$ keV for MOS1 and MOS1, $9.5-12$ keV for PN) count rate evaluated on the whole detector FOV was more than 3σ away from its average value. To achieve a tighter filtering of background flares, we iteratively repeated this process two more times, re-evaluating the average hard-band count-rate and excluding time intervals away more than 3σ from this value. The same procedure was applied to soft $1-5$ keV band restricting the analysis to an annulus with inner and outer radii of 12' and 14', where the emission from the radio galaxy is expected to be small.

We merged data from MOS1, MOS2 and PN detectors from all observations using the MERGE task, to detect the fainter sources that would not be detected otherwise. Sources were detected on these merged images following the standard SAS sliding box task EDETECT_CHAIN that mainly consist of three steps: (i) source detection with local background, with a minimum detection likelihood of 8; (ii) remove sources in step 1 and create a smooth background maps by fitting a 2-D spline to the residual image; (iii) source detection with the background map produced in step 2 with a minimum detection likelihood of 10.

The task EMLDETECT was then used to determine the parameters for each input source by means of a maximum likelihood fit to the input images, selecting sources with a minimum detection likelihood of 15 and a flux in the 0.3−10 keV band larger than 10^{-14} erg cm^{-2} s^{-1} (assuming an energy conversion factor of 1.2×10^{-11} cts cm^2 erg^{-1}). An analytical model of the point spread function (PSF) was evaluated at the source position and normalized to the source brightness. The source extent was then evaluated as the radius at which the PSF level equals half of local background. We finally visually inspected the detected sources and removed evident spurious detections (i. e., at chip borders, in regions of diffuse emission, etc.). We then produced "swiss-cheese" images for each detector array and observation.

As shown in the upper panels of Fig. 18 we clearly detected extended X-ray emission in the merged *XMM-Newton* archival images around each radio galaxy, while in the lower panels of Fig. 18 the surface brightness profiles are also reported.

It is also worth mentioning that we measured the integrated X-ray flux over a circular region of size equal to the maximum extent of the X-ray diffuse emission, evaluated by the surface brightness profiles, and it is in agreement with those values estimated using Eq. (3) and Eq.(4) for all three radio galaxies.

8. SUMMARY AND CONCLUSIONS

We recently carried out an extensive investigation of the RG large-scale environment in the local Universe (i.e., at $z_{src} \leq 0.15$). Our analysis was based on the comparison of different clustering algorithms and on the development of a new method, based on the counts of cosmological neighbors: optical sources lying within 2 Mpc and with a redshift difference $\Delta z \leq 0.005$ with respect to the RG lying at the center of the field examined, a method known as cosmological overdensity. Our study was also based on extremely homogeneous RG catalogs, with uniform radio, infrared and optical data available for all sources, allowing us to distinguish between FR I and FR II or LERG vs. HERG. We found that independently of their radio morphological classification they all appear to live in similar galaxy-rich large-scale environments. The same result, even if less statistically significant, was also obtained while investigating LERG vs HERG environments (M19).

Here we first performed a dedicated analysis to show how cosmological biases and artifacts can affect analyses of RG large-scale environments and how the cosmological overdensity is almost not affected. Then, even if our procedure is dependent by the SDSS selection of spectroscopic targets, it permits us to obtain better estimates of i) the ambient richness ii) the center of the galaxy distribution surrounding target RGs and iii) the redshift difference between central RG and the average values of cosmological neighbors, that seems to be a better estimate of the environmental redshift. We stress the importance of *comparing radio sources in the same redshift bins* to obtain a complete overview of their large-scale environments in particular for procedures not based on spectroscopic redshift estimates.

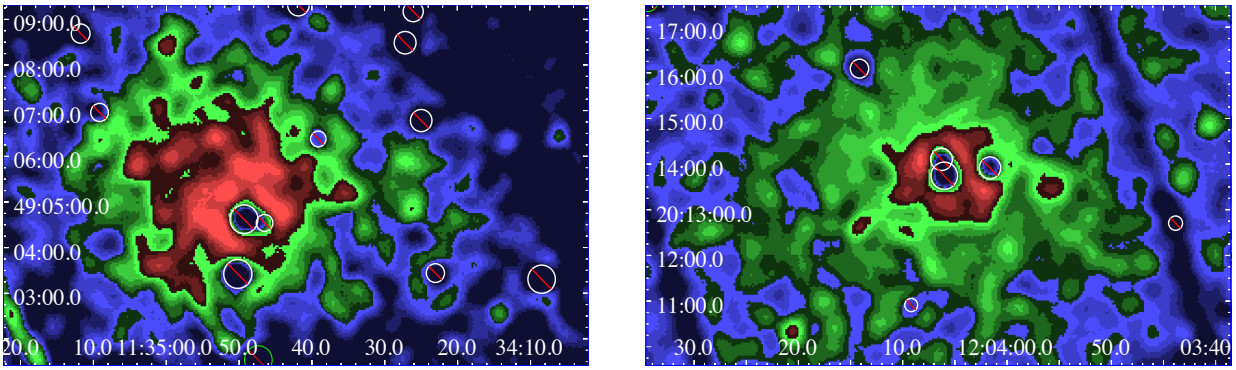


FIG. 18.— The "swiss-cheese" images for two FR Is having XMM-Newton archival observations cut to 5.5 ksec exposure time, namely: SDSS J113359.23+490343.4 (left panel), SDSS J120401.4+201356.3 (right panel). These images show the clear detection of extended X-ray emission around both FR Is using merged XMM-Newtown observations. Images are background and point source subtracted and normalized for the exposure map. Then we also smoothed them with a Gaussian kernel of 8 pixels. White circular regions mark the location of all point sources detected during our data reduction procedure lying in the field.

We also presented an additional statistical test based on the distribution of the median values of the RG population that showed, consistently with our previous analysis, how FR Is and FR IIs live in large-scale environments having environments that are *indistinguishable* on the basis of the statistical analysis we carried out, at all redshifts up to z_{src} =0.15. The lack of a significant number of HERGs (only 14 out of 105 total RGs) listed in the FRIICAT prevent us to draw firm conclusions on the comparison between them and LERGs and thus it was not explored.

In the current paper we also investigated several properties of the RG environments on Mpc scale using the cosmological neighbors distribution and a few parameters derived. Our main results are summarized as follows.

1. The concentration parameter ζ_{cn}, defined as the ratio between the number of cosmological neighbors within 500 kpc and those within 1 Mpc, does not depend by the RG redshift z_{src} and has a distribution that does not depend by the radio classification (i.e., FR I vs. FR II). Typical values of ζ_{cn} are well above 0.25 expected by a uniform distribution of surrounding cosmological neighbors. Consistent results are obtained even when using the number of candidate elliptical galaxies instead of the cosmological neighbors.

2. FR Is and FR IIs have also similar distributions of the standard deviation σ_z of the redshift distribution of the cosmological neighbors as well as their average projected distance d_m^{cn} computed between their position and that of the central RG. This implies that in the redshift range explored the RG environments have similar sizes.

3. When comparing the properties of the cosmological neighbors with those of the central RGs, as the absolute magnitude M_r, the radio power L_R and $[OIII]$ emission line luminosity, we did not find any trend and any difference between FR I and FR II populations.

Finally, we used the σ_z parameter to estimate the velocity dispersion of cosmological neighbors and assume that this is the same of all galaxies belonging to the large-scale environment of both RG populations. Then under the assumption that these RG environments are virialized we estimated the total mass M_{env} present therein, i.e., mass of galaxies plus IGM plus dark matter content.

Thanks to the correlations between M_{env} and the X-ray luminosity L_X of the IGM we also computed the expected values necessary to draw the feasibility of future X-ray campaigns and/or pave the path to what eROSITA will be able to detect in the near future. Given the same distribution of σ_z and the lack of any trend with this parameter with those of the central radio galaxies (i.e., M_r, L_R and $L_{[OIII]}$) the same situation occurs with the derived quantities: M_{env} and L_X of their large-scale environments. However, the estimates of X-ray fluxes confirm that X-ray counterpart of the groups and clusters of galaxies around FRICAT and FRIICAT sources should not to be detected in the ROSAT all sky survey demanding to *XMM-Newton* and *Chandra* facilities to get a complete view of their large-scale environments. Finally, we reduced and analyzed *XMM-Newton* observations of two FR I radio galaxies, cutting the total exposure time to 5.5 ksec, to show that a clear detection of galaxy clusters around them can be easily achieved with snapshot observations.

APPENDIX

FIGURES & TABLES

We did not find any trend between the environmental parameters: d_m^{cn} and σ_z radio galaxy parameters as M_R, L_R, $L_{[OIII]}$, but all plots are indeed shown in this Appendix A in Fig. 19, Fig. 20 and Fig. 21, respectively.

We then reported here in Table 3 all parameters estimated for each RG analyzed.

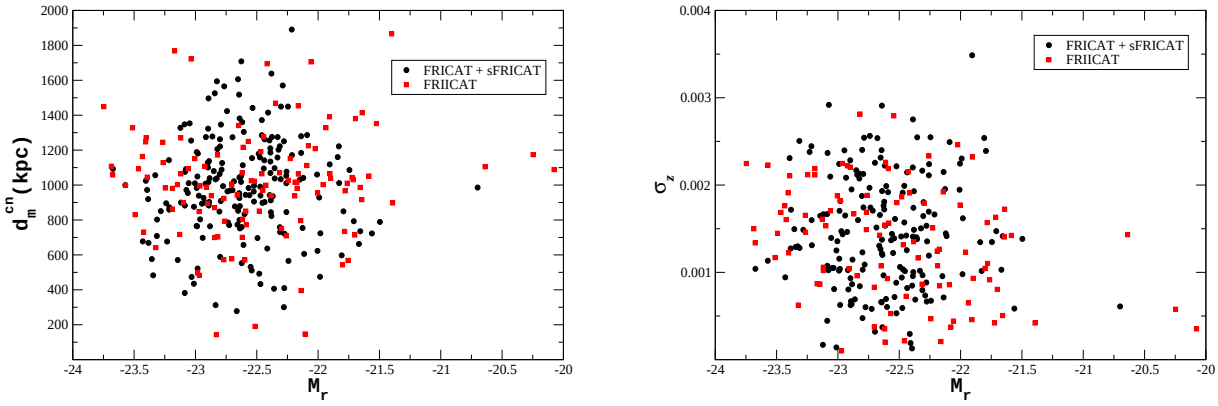


FIG. 19.— Left panel) the scatter plot of the average projected distance d_m^{cn} of the distribution of cosmological neighbors as function of the absolute magnitude M_r of the central radio galaxy for both FR Is (black circles) and FR IIs (red squares). No neat trend or correlation is found between these two parameters. Right panel) the standard deviation σ_z of redshift distribution estimated using all cosmological neighbors lying within 2 Mpc as function of M_r of the central RG. Again FR Is are marked as black circles while FR IIs as red squares.

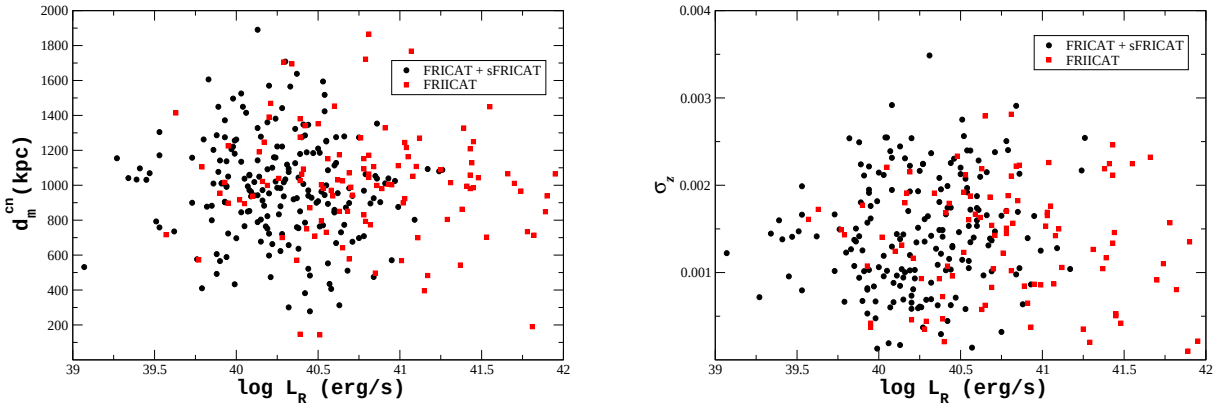


FIG. 20.— Same as left panel and right panel of Fig. 19 but as function of the radio luminosity, respectively.

We thank the anonymous referee for useful and valuable comments that led to improvements in the paper. In particular, all her/his statistical notes that have been implemented in the revised version of the manuscript. F. M. wishes to thank Dr. C. C. Cheung for their valuable discussions on this project initially planned during the IAU 313 on the Galapagos islands. This work is supported by the "Departments of Excellence 2018 - 2022" Grant awarded by the Italian Ministry of Education, University and Research (MIUR) (L. 232/2016). This research has made use of resources provided by the Compagnia di San Paolo for the grant awarded on the BLENV project (S1618_L1_MASF_01) and by the Ministry of Education, Universities and Research for the grant MASF_FFABR_17_01. This investigation is supported by the National Aeronautics and Space Administration (NASA) grants GO6-17081X and GO9-20083X. F.M. acknowledges financial contribution from the agreement ASI-INAF n.2017-14-H.0. Funding for SDSS and SDSS-II has been provided by the Alfred P. Sloan Foundation, the Participating Institutions, the National Science Foundation, the U.S. Department of Energy, the National Aeronautics and Space Administration, the Japanese Monbukagakusho, the Max Planck Society, and the Higher Education Funding Council for England. The SDSS Web Site is http://www.sdss.org/. The SDSS is managed by the Astrophysical Research Consortium for the Participating Institutions. The Participating Institutions are the American Museum of Natural History, Astrophysical Institute Potsdam, University of Basel, University of Cam- bridge, Case Western Reserve University, University of Chicago, Drexel University, Fermilab, the Institute for Advanced Study, the Japan Participation Group, Johns Hopkins University, the Joint Institute for Nuclear Astrophysics, the Kavli Institute for Particle Astrophysics and Cosmology, the Korean Scientist Group, the Chinese Academy of Sciences (LAMOST), Los Alamos National Laboratory, the Max- Planck-Institute for Astronomy (MPIA), the Max-Planck- Institute for Astrophysics (MPA), New Mexico State University, Ohio State University, University

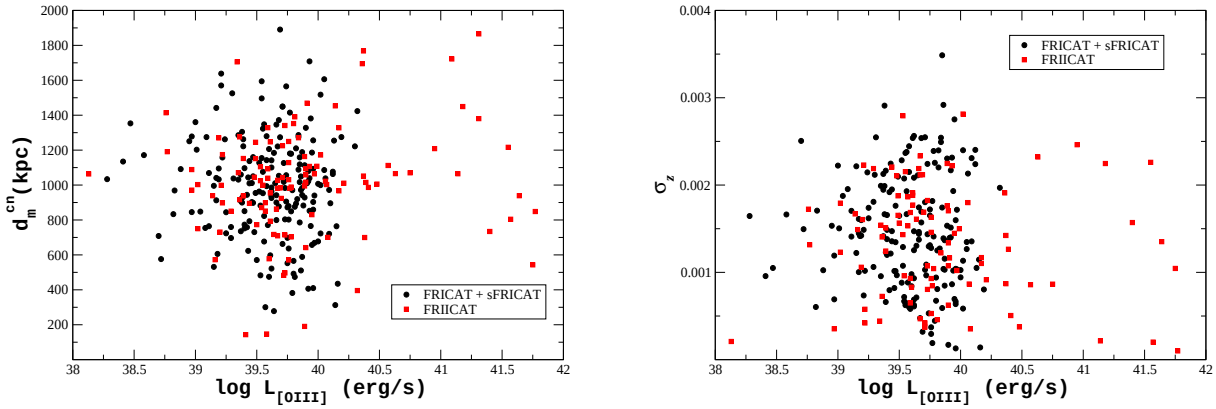


FIG. 21.— Same as left panel and right panel of both Fig. 19 and Fig. 20 but as function of the [OIII] emission line luminosity, respectively.

TABLE 3
ENVIRONMENTAL PARAMETERS FOR THE FRICAT AND THE FRIICAT (FIRST 10 LINES)

SDSS name	Radio Class	z_{src}	Δz	d_{proj} (kpc)	N_{cn}^{500}	N_{cn}^{1000}	N_{cn}^{2000}	ζ_{cn}	$< z_{cn} >$	σ_z	d_{proj}^{cn} (kpc)	d_m^{cn} (kpc)	σ_v (km/s)	M_{env} $M_\odot$	F_X erg/cm^{2}s^{-1}
J073014.37+393200.4	FRI	0.142	5.3E-4	450.42	1	4	6	0.25	0.141	0.00082	207.56	902.48	215.61	11.86	-13.18
J073505.25+415827.5	FRI	0.087	5.2E-4	161.92	3	4	10	0.75	0.088	0.00061	758.00	985.60	168.04	11.64	-13.05
J073719.18+292932.0	FRI	0.111	8.1E-4	159.92	1	1	5	1.00	0.108	0.00161	826.91	1441.76	436.15	12.47	-12.07
J074125.85+480914.3	FRI	0.12	-	-	0	0	1	-	0.115	-	1890.54	1890.55	-	-	-
J074351.25+282128.0	FRI	0.106	3.0E-4	63.64	4	4	9	1.00	0.106	0.00211	258.80	1010.41	572.42	12.71	-11.69
J075221.83+333348.9	FRII	0.14	1.7E-4	111.63	2	2	4	1.00	0.138	0.00143	140.75	943.39	375.43	12.34	-12.47
J075309.91+355557.1	FRI	0.113	4.5E-4	180.50	2	4	5	0.50	0.113	0.00097	229.58	730.53	260.57	12.02	-12.73
J075506.67+262115.9	FRI	0.123	-	-	0	0	1	-	0.123	-	1274.66	1274.66	-	-	-
J075529.95+520450.6	FRII	0.14	-	-	0	0	0	-	-	-	-	-	-	-	-
J075628.78+501716.3	FRII	0.134	-	-	0	0	2	-	0.133	0.00087	322.70	1768.24	230.16	11.91	-13.04

Col. (1): SDSS name.
Col. (2): Radio class to distinguish between source belonging to the FRICAT and the FRIICAT.
Col. (3): source redshift.
Col. (4): Absolute value of the redshift difference between the RG and the closest galaxy cluster in the T12 catalog.
Col. (5): Physical distance between the RG and the closest galaxy cluster in the T12 catalog. This is computed at the z_{src} of the central RG.
Col. (6,7,8): Number of cosmological neighbors within 500, 1000 ad 2000 kpc, respectively, estimated at the z_{src} of the central radio galaxy.
Col. (9): The concentration parameter ζ_{cn}.
Col. (10): The average redshift of the cosmological neighbors in 2 Mpc.
Col. (11): The standard deviation of the redshift distribution for the cosmological neighbors within 2 Mpc.
Col. (12): Physical distance between the central RG and the average position of the cosmological neighbors within 2 Mpc. This is computed at the z_{src} of the central RG.
Col. (13): Average distance of the cosmological neighbors within 2 Mpc.
Col. (14): Velocity dispersion of the cosmological neighbors located in 2 Mpc.
Col. (15): Environmental mass estimated from the velocity dispersion.
Col. (16): X-ray flux estimated from the velocity dispersion.

of Pittsburgh, University of Portsmouth, Princeton University, the United States Naval Observatory, and the University of Washington. TOPCAT and STILTS astronomical software (Taylor 2005) were used for the preparation and manipulation of the tabular data and the images.

REFERENCES

Abell, G. O., Corwin, H. G. Jr., Olowin, O. P. 1989 ApJS, 70, 1
Ahn, C. P., Alexandroff, R., Allende Prieto, C., Anderson, Scott F., Anderton, T. et al. 2012 ApJS, 203, 21
Baldi, Ranieri D.; Capetti, Alessandro; Giovannini, Gabriele 2015 A&A, 576A, 38
Baldi, R. D.; Capetti, A.; Massaro, F. 2018 A&A, 609A, 1
Belsole, E.; Worrall, D. M.; Hardcastle, M. J.; Croston, J. H. 2007 MNRAS 381, 1109
Bennett, C. L., Larson, D., Weiland, J. L., Hinshaw, G. 2014 ApJ 794, 135
Berlind, A. A. et al. 2006 ApJS, 167, 1
Best, P. N. 2004 MNRAS 351, 70
Best, P. N.; Heckman, T. M. 2012 MNRAS 421, 1569
Biviano A. 2000 IAP meeting "Constructing the Universe with Clusters of Galaxies", Paris, France, July 2000, Florence Durret & Daniel Gerbal Eds.,
Blanton, E. L.; Gregg, M. D.; Helfand, D. J.; Becker, R. H.; White, R. L. 2000 ApJ, 531, 118
Blanton, E. L.; Gregg, M. D.; Helfand, D. J.; Becker, R. H.; Leighly, K. M. 2001 AJ, 121, 2915
Capetti, A., Massaro, F., Baldi, R. D. 2017 A&A 598A, 49
Capetti, A., Massaro, F., Baldi, R. D. 2017 A&A 601A, 81
Ching, J. H. Y.; Croom, S. M.; Sadler, E. M.; Robotham, A. S. G.; Brough, S. et al. 2017 MNRAS 469, 4584
Clerc, N.; Merloni, A.; Zhang, Y. -Y.; Finoguenov, A.; Dwelly, T. et al. 2016 MNRAS 463, 4490

Condon, J. J., Cotton, W. D., Greisen, E. W., Yin, Q. F., Perley, R. A., Taylor, G. B., & Broderick, J. J. 1998, AJ, 115, 1693
Croston, J. H.; Hardcastle, M. J.; Birkinshaw, M.; Worrall, D. M.; Laing, R. A. 2008 MNRAS, 386, 1709
Danese, L., de Zotti, G., di Tullio, G., 1980 A&A, 82, 322
D'Abrusco, R.; Longo, G.; Walton, N. A. 2009 MNRAS 396, 223
D'Agostini, G. 2003 "Bayesian reasoning in data analysis: A critical introduction", World Scientific Publishing, 2003
Ebeling, H.; Edge, A. C.; Bohringer, H.; Allen, S. W.; Crawford, C. S.; Fabian, A. C.; Voges, W.; Huchra, J. P. 1998 MNRAS 301, 881
Eke, V. R 2004 MNRAS, 348, 866
Evans, D. A.; Worrall, D. M.; Hardcastle, M. J.; Kraft, R. P.; Birkinshaw, M. 2006 ApJ, 642, 96
Fadda, D.; Girardi, M.; Giuricin, G.; Mardirossian, F.; Mezzetti, M. 1996 ApJ, 473, 670
Fanaroff, B. L, Riley, J. M. 1974 MNRAS 167, 31
Gendre M. A., Best, P. N., Wall, J. V. and Ker, L.M. 2013 MNRAS 430, 3086
Girardi, M.; Biviano, A.; Giuricin, G.; Mardirossian, F.; Mezzetti, M. 1993 ApJ, 404, 38
Gladders, M. D., Lopez-Cruz, O., Yee, H. K. C. & Kodama, T. 1998, ApJ, 501, 571
Gladders, Michael D.; Yee, H. K. C. 2000 ApJ 120, 2148
Haas, M. R., Schaye, J., Jeeson-Daniel, Akila 2012 MNRAS 419, 2133
Hardcastle, M. J.; Worrall, D. M. 2000 MNRAS, 319, 562
Helfand, D. J., White, R. L., Becker, R. H. 2015 ApJ, 801,26
Hill, G. J. and Lilly, S. J. 1991 ApJ 367, 1
Hine, R. G.; Longair, M. S. 1979 MNRAS 188, 111
Huchra J. P., Geller M. J., 1982, ApJ, 257, 423
Ineson, J.; Croston, J. H.; Hardcastle, M. J.; Kraft, R. P.; Evans, D. A.; Jarvis, M. 2013 ApJ 770, 136
Ineson, J.; Croston, J. H.; Hardcastle, M. J.; Kraft, R. P.; Evans, D. A.; Jarvis, M. 2015 MNRAS 453, 2682
Laing, R. A.; Jenkins, C. R.; Wall, J. V.; Unger, S. W. 1994 The First Stromlo Symposium: The Physics of Active Galaxies. ASP Conference Series, Vol. 54, 1994, G.V. Bicknell, M.A. Dopita, and P.J. Quinn, Eds., p.201
Lintott, C. J., Schawinski, K., Slosar, A., Land, K., Bamford, S. et al. 2008 MNRAS 389, 1179
Lloyd-Davies, E. J.; Romer, A. Kathy; Mehrtens, Nicola; Hosmer, Mark; Davidson, Michael et al. 2011 MNRAS 418, 14
Massaro, F., D'Abrusco, R., Ajello, M. et al. 2011 ApJ, 740L, 48
Massaro, F., Tremblay, G. R., Harris, D. E. et al. 2012 ApJS, 203, 31
Massaro, F., D'Abrusco, R., Paggi, A. et al. 2013a ApJS, 209, 10
Massaro, F., Harris, D. E., Liuzzo, E. et al. 2015 ApJS, 220, 5
Massaro, F., Missaglia, V., Stuardi, C., Harris, D. E., Kraft, R. P. et al. 2018 ApJS, 234, 7
Massaro, F., N. Álvarez-Crespo, N., Capetti, A., Baldi, R. D., Pillitteri, I., Campana, R., Paggi, A., 2019 ApJS, 240, 2
Mehrtens, Nicola; Romer, A. Kathy; Hilton, Matt; Lloyd-Davies, E. J.; Miller, Christopher J. et al. 2012 MNRAS 423, 1024
Mingo, B.; Hardcastle, M. J.; Croston, J. H.; Dicken, D.; Evans, D. A.; Morganti, R.; Tadhunter, C. 2014 MNRAS, 440, 269
Mingo, B.; Hardcastle, M. J.; Ineson, J.; Mahatma, V.; Croston, J. H.; Dicken, D.; Evans, D. A.; Morganti, R.; Tadhunter, C. 2017 MNRAS, 470, 2762
Miraghaei, H. and Best, P. N. 2017 MNRAS 466 4346
Moore, B., Frenk, C. S., White, S. D. M. 1993 MNRAS, 261, 827
Nevalainen, J.; Markevitch, M.; Lumb, D. 2005 ApJ 629, 172
Prestage, R. M.; Peacock, J. A. 1988 MNRAS 230, 131
Reiprich, T. H., B´ohringer H. 1999 AN, 320, 296
Richards, Gordon T.; Nichol, Robert C.; Gray, Alexander G.; Brunner, Robert J.; Lupton, Robert H. et al. 2004 ApJS 155, 257
Rines, Kenneth; Geller, Margaret J.; Diaferio, Antonaldo; Kurtz, Michael J. 2013 ApJ, 767, 15
Sabater, J.; Best, P. N.; Argudo-Fernàndez, M. 2013 MNRAS 430 ,638
Stuardi, C., Missaglia, V., Massaro, F., Ricci, F., Liuzzo, E. et al. 2018 ApJS, 235, 32
Tago, E.; Saar, E.; Tempel, E.; Einasto, J.; Einasto, M.; Nurmi, P.; Heinämäki, P. 2010 A&A, 514A, 102
Taylor M. B., 2005, ASPC, 347, 29
Tasse, C.; Best, P. N.; Röttgering, H.; Le Borgne, D. 2008 A&A, 490, 893
Tempel, E.; Tago, E.; Liivamägi, L. J. 2012 A&A 540A,106
Visvanathan, N., & Sandage, A. 1977, ApJ, 216, 214
White, R. L., Becker, R. H., Helfand, D. J.; Gregg, M. D. 1997 ApJ 475, 479
Wilkes, Belinda J.; Kuraszkiewicz, Joanna; Haas, Martin; Barthel, Peter; Leipski, Christian; Willner, S. P. et al. 2013 ApJ, 773, 15
Wing, Joshua D.; Blanton, Elizabeth L. 2011 AJ 141, 88
Worpel, Hauke; Brown, Michael J. I.; Jones, D. Heath; Floyd, David J. E.; Beutler, Florian 2013 ApJ 772, 64
Worrall, D. M.; Birkinshaw, M. 2000 ApJ, 530, 719
Wright, E. L., et al. 2010 AJ, 140, 1868
Zhang, Y. Y., Andernach, H., Caretta, C. A., Reiprich, T. H., B´ohringer, H., Puchwein, E., Sijacki, D. & Girardi, M. 2011 A&A, 526, A105
Zirbel, E. L. 1997 ApJ 476, 489